

Load-Bearing Performance of a Reinforced Fill Structure with Pile Penetration

Qiang Ma ^{1,*} , Hanlong Yu ¹, Yicong Yang ^{2,*} and Lei Xi ¹

¹ School of Civil Engineering, Architecture and Environment, Hubei University of Technology, Wuhan 430068, China; 15527078067@163.com (H.Y.); leixi@whut.edu.cn (L.X.)

² Sinohydro Bureau 8 Co., Ltd., No.8, Changqing Road, Tianxin District, Changsha 410004, China

* Correspondence: maqiang927@163.com (Q.M.); yangyc-baju@powerchina.cn (Y.Y.);

Tel.: +86-134-1957-0653 (Q.M.); +86-180-7106-4510(Y.Y.)

Abstract: Reinforcement soil slope with pile penetration is a new load bearing structure, which has a complex working mechanism, but few studies have been carried out. This paper aims to investigate the stability characteristics of this structure using model tests. The study investigates the lateral displacement and pile bending moment caused by vertical loads and evaluates the influence of different factors, including the structure type (such as pile, cap of pile, and reinforcement material), number of reinforcing layers, spacing of reinforcement material, pile length, and slope rate on the load-carrying capacity of the pile penetration fill-reinforced load-bearing structure. The findings suggest that within a certain range, increasing the pile length and number of reinforcing layers, the limiting effect of the pile on the lateral displacement in the middle and at the bottom of the slope of the pile-penetrating reinforced structure is enhanced, which can reduce the extreme value of the bending moment and make the distribution of the bending moment of the pile more reasonable. The lateral limiting effect on the soil body can be maximized by appropriate reinforcement spacing. Within a certain range, the slope rate is reduced, which can reduce the extreme value of the bending moment, make the bending moment distribution of the pile more reasonable, and avoid the phenomenon of the localized force concentration of the pile.

Keywords: pile penetration structure; vertical load; model test; stability



Citation: Ma, Q.; Yu, H.; Yang, Y.; Xi, L. Load-Bearing Performance of a Reinforced Fill Structure with Pile Penetration. *Appl. Sci.* **2024**, *14*, 4065. <https://doi.org/10.3390/app14104065>

Academic Editor: Tiago Miranda

Received: 8 April 2024

Revised: 2 May 2024

Accepted: 6 May 2024

Published: 10 May 2024



Copyright: © 2024 by the authors. Licensee MDPI, Basel, Switzerland. This article is an open access article distributed under the terms and conditions of the Creative Commons Attribution (CC BY) license (<https://creativecommons.org/licenses/by/4.0/>).

1. Introduction

In various geotechnical engineering projects, piles are often employed to withstand lateral loads. These piles can be classified into two types in practical application: active piles and passive piles. Active piles primarily bear the top load to support upper structures, such as bridges [1–6]. In contrast, passive piles endure the primary load along their length due to soil pressure [7–9]. The use of piles to stabilize slopes falls under the category of passive piles. Given the complexity of passive piles, analyzing and designing passive piles on slopes is a challenging task. Zomorodian et al. (2011) [10] conducted model tests to investigate the factors affecting slope stability, including the position of pile foundations, geological characteristics, slope angle, depth of embedded piles, and pile structure methods. The aim of their research was to prevent disasters, such as landslides and collapses, and to ensure the stability of sloping pile foundations. Pierson et al. (2009) [11] verified the feasibility of using a pile foundation in reinforced backfill to improve the horizontal bearing performance of the structure through experiments. Sawwaf et al. (2006) [12] investigated the horizontal load-bearing capacity of piles near geogrid-reinforced slopes. Their study showed that reinforcing the soil slope can improve the horizontal load-bearing capacity of internal piles. The proximity of the piles to the slope also affects the extent to which the load capacity is increased. Therefore, in order to clear the effect of soil reinforcement on slope stability, researchers have conducted indoor modeling tests on the bearing capacity of the bar foundation on sandy reinforced soil slopes. These tests have considered various

factors, such as different boundary conditions, geotechnical reinforcement lengths, the number of layers of reinforcement, and the vertical spacing of reinforcement [13]. It has been shown that reducing the spacing between reinforcing layers can enhance the slope-bearing capacity. Additionally, the location of the peak strain on the slope will vary with the changes in the applied load [14]. Choudhary et al. (2010) [15] conducted indoor model tests to investigate the characteristics of fly ash geogrid slopes under top-loading conditions. The study revealed that geogrids can improve the load-settlement performance and enhance the maximum bearing capacity of slopes. Moreover, the analysis of the percolation performance in reinforced slopes demonstrated that geotextiles effectively enhance the stability of low-permeability slopes. Additionally, it was found that the reinforcement material layer placed in the lower half of the slope significantly dissipates pore water pressure [16]. Some scholars have also utilized centrifuge model tests to analyze the stability of geotextile-reinforced slopes. Gil et al. (2013) [17] conducted a study combining finite element analysis with model tests to investigate the effect of fly ash as roadbed material on reinforced slopes. The results showed that increasing the number of reinforcement layers within a certain range improves the slope-bearing capacity.

However, existing studies have not yet conducted an in-depth study on the force characteristics of slope piles under geogrid reinforcement conditions for such a complex condition, where the mechanism of action between the various components of the structure is complicated. The structure method of the reinforced fill structure with pile penetration proposed in this study is a novel technique. It can more comprehensively show the influence of the combined action of various factors. The structure comprises reinforced soil, slopes, and piles, and there are various factors that influence the structural stability under loads. Therefore, the model tests under 17 different conditions to investigate the bearing and reinforcement characteristics of the structures were conducted in this study.

2. Experimental Materials

2.1. Sand Sample

To simulate the soil more accurately, sand used for this experiment was obtained from river sand in Wuhan, Hubei Province, China. Prior to usage, the river sand was dried in an oven to minimize the impact of moisture on the experimental results. The temperature in the oven was kept at 45 degrees Celsius. Following the principles of similarity theory, geotechnical tests were performed on the river sand. Table 1 presents the physical properties of the sand, while Figure 1 depicts its particle size distribution curve.

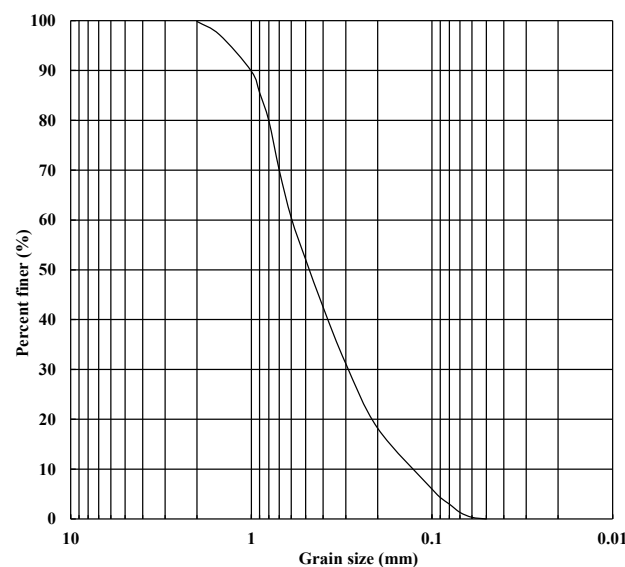


Figure 1. Gradation of sand particles.

Table 1. Indicators of physical properties of sandy soils (Tolerance within 5%).

$\gamma/(\text{kg/m}^3)$	G_s	e	$\omega/\%$	C_u	C_c	$\varphi/(\text{°})$
16.81	2.67	0.51	0.18	3	0.75	30

2.2. Reinforcement Material

The selection of geogrid similar materials needs to meet the conditions of mechanical similarity and geometric similarity at the same time. Therefore, plain knitted cotton fabric was used as reinforcement in the test, and the thickness was about 0.2 mm. According to the literature [18,19], the material properties of plain knitted cotton fabric were studied. The material parameters of plain knitted cotton fabric are shown in Table 2.

Table 2. Material parameters of cotton ribbed material [18].

$\rho/(\text{kg/m}^{-3})$	σ_y/MPa	E/MPa	E_t/MPa	Poisson Ratio ν
900	31.24	254	0	0.3

2.3. Piles

(1) Pile

Currently, commonly used materials for model test piles include wood [20,21], organic glass [18,22], three-type polypropylene pipe (PPR pipe) [23], PVC pipe [24], and others. Previous studies [25] have indicated that PVC pipe is a favorable choice for model test pile materials due to its high strength, ease of processing, and other advantages. Considering the specific characteristics of this experiment, PVC pipe was selected as the material for the model test pile. The material parameters for the pile are detailed in Table 3, based on research on PVC pipe material properties [24].

Table 3. Pile material parameters [24].

Pile Materials	Pile Length L/cm	External Diameter D/m	Inside Diameter D/m	Wall Thickness T/m	Modulus of Elasticity E/GPa	Poisson Ratio ν
PVC	60	0.05	0.046	0.002	3.7527	0.39
PVC	50	0.05	0.046	0.002	3.7527	0.39
PVC	55	0.05	0.046	0.002	3.7527	0.39
PVC	65	0.05	0.046	0.002	3.7527	0.39

To simulate the frictional resistance on the surface of the original pile, the model pile surface is coated with a mixture of poly-amide resin and epoxy resin, onto which sieved medium-coarse sand was applied. Make the sand stick to the surface of the PVC pipe to simulate the pile roughness.

(2) Bottom of pile

A 10 mm-thick plexiglass of the same size as the outside diameter of the pile was used at the bottom of the model pile and sealed with transparent tape to avoid soil ingress into the model pile.

(3) Cap of pile

The test was conducted by using a Plexiglas sheet to simulate the cap of pile with the size of 0.2 m \times 0.2 m \times 0.01 m, which was connected to the pile by 502 adhesive to form a pipe pile with a cap of pile.

To account for boundary effects, a minimum distance of 400 mm was maintained between the model piles and the boundaries of the model box. This distance exceeds the requirement of $3D = 3 \times 63 = 189$ mm [26,27]. Therefore, the size effect caused by the model box can be considered negligible.

2.4. Backfilling Requirements

Manual tamping was carried out using the layered fill method, and the fill control indicators measured through tamping and percussion tests are shown in Table 4.

Table 4. Control index for fill placement.

Relaxation Factor	Loose Lay Thickness/cm	Compacted Thickness/cm	Number of Compaction Passes	Compaction/%
1.4	14	10	8	≥ 91

3. Experimental Apparatus

3.1. Experimental Model Box

The experiment was carried out in a model box of 2000 mm in length, 800 mm in width, and 760 mm in height. On the front of the model box, 20 mm-thick toughened glass was used to facilitate the observation of model deformation. Marking lines on glass panels was used to facilitate the observation of slope deformation on embankment slopes. Lubricant was used on the sidewalls during the model-making process to decrease friction between the soil and walls, thus reducing boundary effects. For more details, please refer to Figure 2.

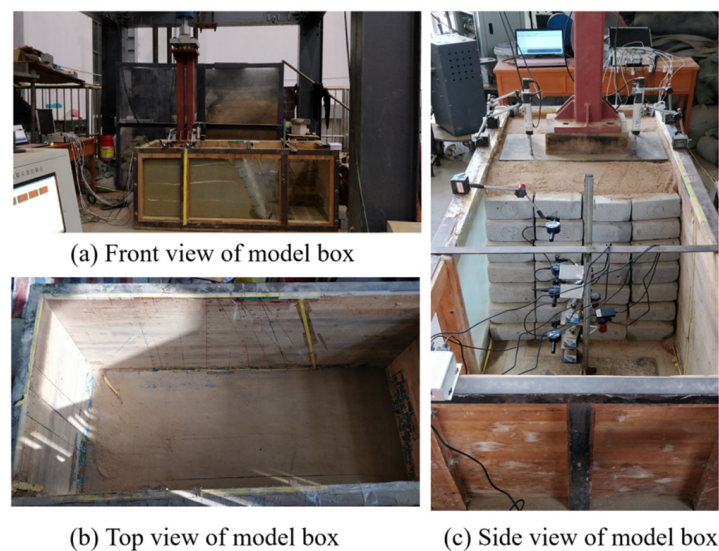


Figure 2. Photograph of model box.

3.2. Loading Plate

To ensure uniform loading, a steel plate with a dimension of 760 mm \times 440 mm \times 15 mm (length \times width \times height) was selected as the loading plate. It was placed directly beneath the vertical actuator. Additionally, two square wooden blocks with a dimension of 380 mm \times 160 mm \times 120 mm (length \times width \times height) were placed on the loading plate to simulate sleepers.

3.3. Loading Device

The loading device used in this study is a frame testing machine developed by the Huaxi Institute of Geotechnical Instruments at Sichuan University. As shown in Figure 3 this device ensures that a constant vertical load is applied during the vertical settlement process of the model. It is fixed at the upper end of the overhead reaction frame, which consists of crossbeams and columns.

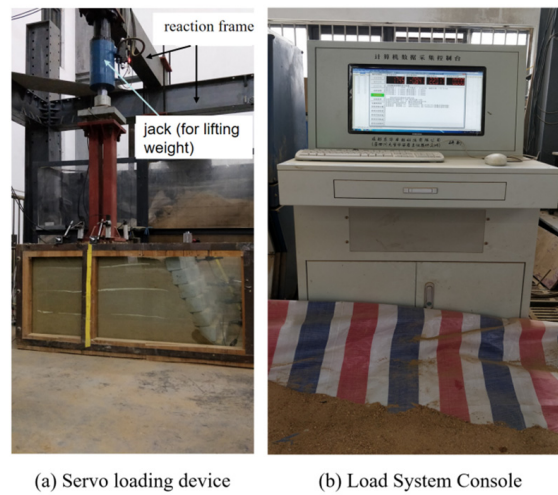


Figure 3. Frame tester loading picking control device.

3.4. Measurement Components and Layout of Measuring Points

The main measuring elements required for the test include micro strain gauges, a miniature earth pressure box, and digital percent gauges, and the acquisition equipment is the TST3826E Static Strain Test Analyzer (Jiangsu Test Electronic Equipment Manufacturing Co. CHINA, Jingjiang, China). The miniature earth pressure box (M1–M12) is spread flat in the soil layer, and the strain gauge (1–10) sticks to the surface of the pile. The specific parameters for the testing components can be found in Table 5, and the reinforcements are spaced 200 mm apart. The layout of these components is illustrated in Figure 4.

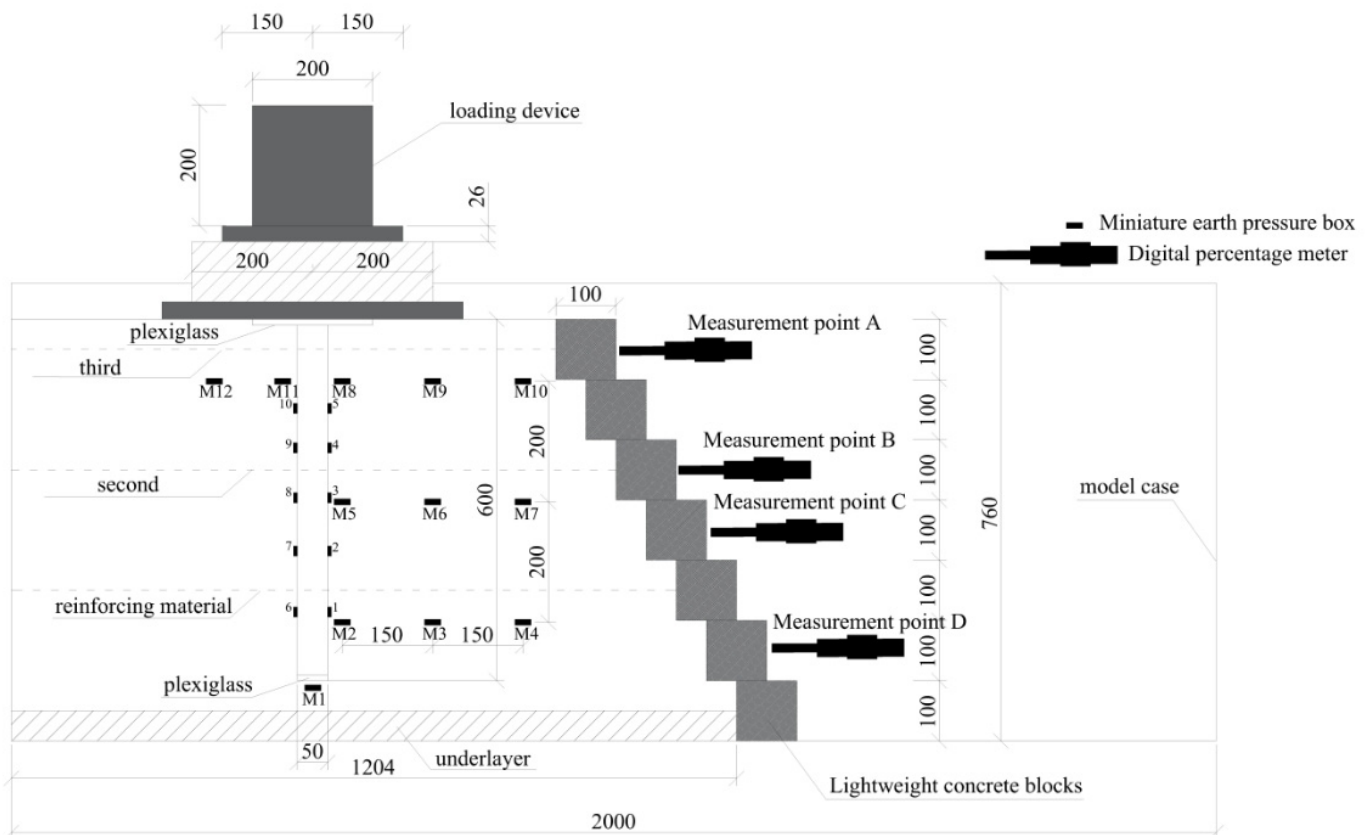


Figure 4. Schematic diagram of model size and instrument arrangement (unit: mm).

Table 5. Test element parameters.

Name	Model	Range	Precision
Miniature earth pressure box (M1–M12)	XB-151	6 MPa	0.001 MPa
Taiwan EEE digital percent gauges	BFQ-350A	0–50	0.01 mm
strain gauge (1–10)	BX120-1AA	20,000 $\mu\epsilon$	1 $\mu\epsilon$

4. Test Program

4.1. Test Conditions

To investigate the impact of different structural types (pile, cap of pile, reinforcement), various pile diameters, different numbers of reinforcement layers, varying stiffnesses of reinforcements, different pile lengths, and different reinforcement spacings on the load-bearing characteristics and reinforcement effects of structures, indoor model experiments were conducted under planar strain conditions. Only single piles were considered for the test. The test conditions are shown in Table 6.

Table 6. Reinforced fill structure with pile penetration model test conditions.

Working Condition	Number of Reinforcement Layers n	Reinforcement Spacing/cm	Pile Length/cm	Cap of Pile	Slope Rate	Reinforcing Material
1	none	none	none	none	0.4	none
2	3	20	none	none	0.4	Flat grain cotton cloth
3	none	none	60	have	0.4	none
4	3	20	60	none	0.4	Flat grain cotton cloth
5	3	20	60	have	0.4	Flat grain cotton cloth
6	2	20	60	have	0.4	Flat grain cotton cloth
7	1	20	60	have	0.4	Flat grain cotton cloth
8	3	20	60	have	0.2	Flat grain cotton cloth
9	3	20	60	have	0.6	Flat grain cotton cloth
10	3	20	60	have	0.4	Geogrid
11	3	20	60	have	0.4	Geotechnical Cloth
12	3	20	50	have	0.4	Flat grain cotton cloth
13	3	20	55	have	0.4	Flat grain cotton cloth
14	3	20	65	have	0.4	Flat grain cotton cloth
15	2	10	60	have	0.4	Flat grain cotton cloth
16	2	30	60	have	0.4	Flat grain cotton cloth
17	2	40	60	have	0.4	Flat grain cotton cloth

4.2. Loading Method

Prior to loading, all equipment readings were checked for correctness, and the digital percentile reading was zeroed. When loading, the static strain collector and the digital display meter synchronously collect the corresponding data. After each level of vertical loading is completed, observe the corresponding vertical load value, displacement value, and strain value through the data acquisition system of the loading device and the digital percentile meter, when the reading is stable, read and record the data manually at the same time (in order to facilitate the analysis and processing of the test data in the later stage), and then carry out the next level of loading, repeat the above steps, step by step, and incrementally increase the vertical load applied until the test loading termination conditions are reached.

After each group of tests reaches the loading termination condition, the test ends immediately. After saving the test data in the data-acquisition system, the measuring equipment was turned off, the external equipment was removed, and the sand, soil pressure box, reinforcement material and model piles were excavated layer by layer and observed for damage.

During loading, data collection was synchronized between the static strain acquisition device and the digital displacement gauge. After each level of vertical load was completed,

the corresponding values of the vertical load, displacement, and strain were observed using the data-acquisition system of the loading device and the digital displacement gauge.

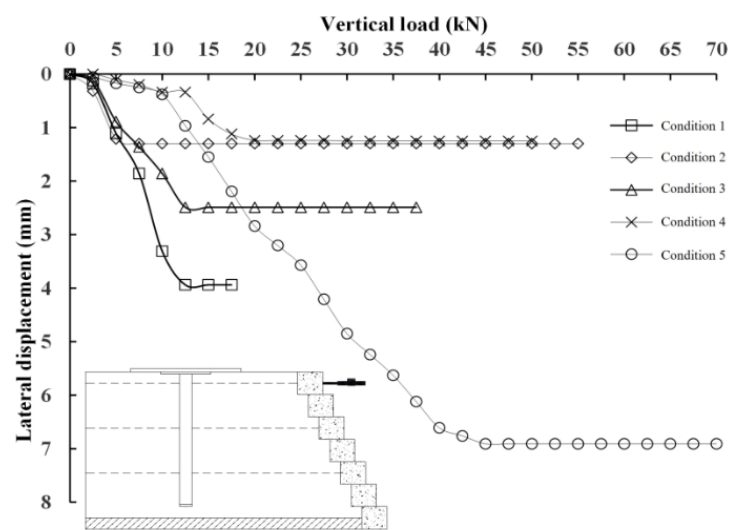
5. Analysis of Results

5.1. Lateral Displacement Analysis

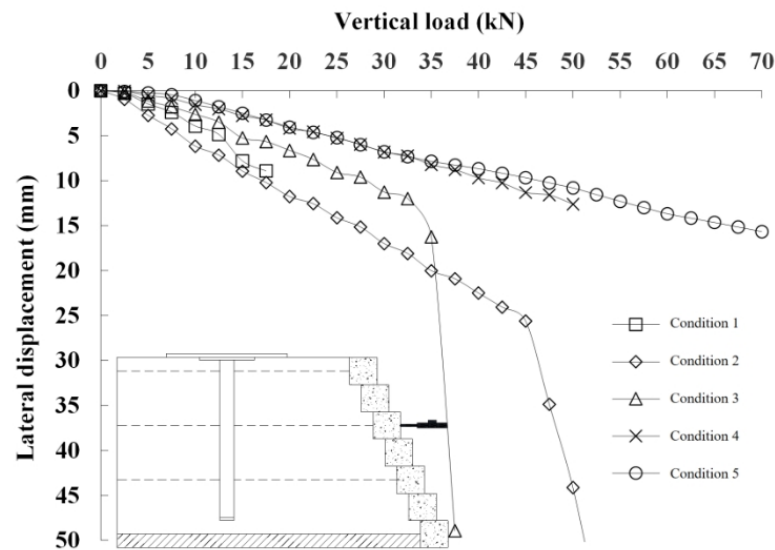
The slope surface was equipped with four digital percentile gauges to measure the lateral displacement at different points. These points include apex A, midpoints B and C, and bottom point D. Measurements were taken at each loading level.

5.1.1. Impact of Different Structure Types

The vertical load–lateral displacement curves for different structural types are shown in Figure 5. The corresponding lateral displacements for different structural types at the ultimate load of 17.5 kN for the pure sand structure are detailed in Table 7.

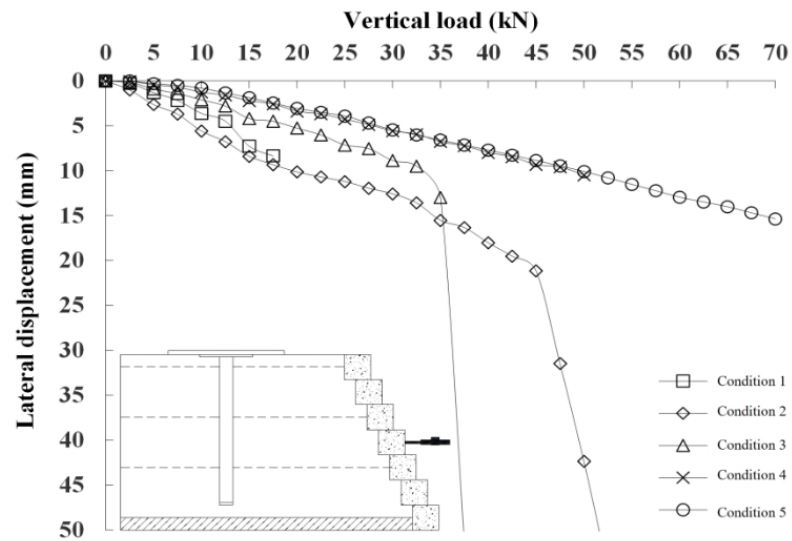


(a) Measurement point A at the top of the slope

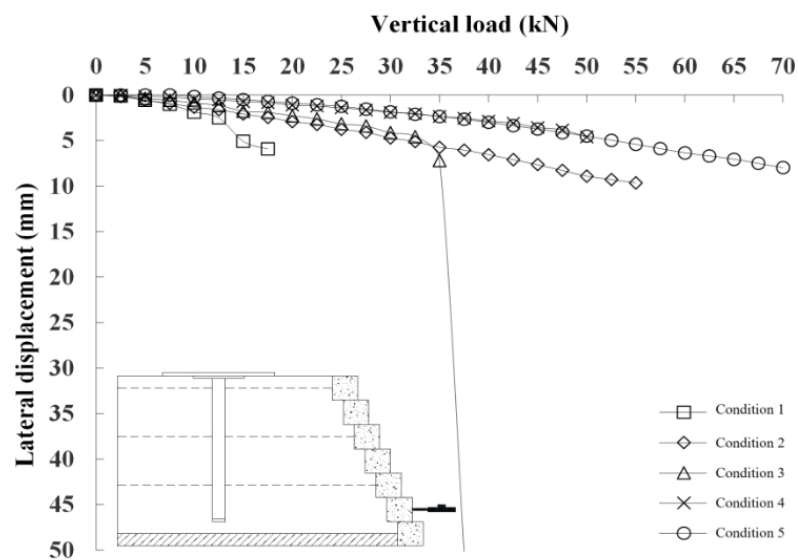


(b) Measurement point B in the middle of the slope

Figure 5. Cont.



(c) Measurement point C in the middle of the slope



(d) Point D at the bottom of the slope.

Figure 5. Vertical load–lateral displacement curves for different structure types.

Table 7. Lateral displacements for different structural types (at a vertical load of 17.5 kN).

Condition	Structure Type	Vertical Load Is the Horizontal Displacement Corresponding to 17.5 kN/mm			
		Slope Bottom D Station	In the Slope C Station	In the Slope B Station	Top of Slope A Station
1	Sand	5.92	8.34	8.93	3.94
2	Flat grain cotton cloth	2.46	9.32	10.21	1.30
3	Pile	1.92	4.48	5.66	2.49
4	Both plain cotton cloth and pile (no cap of pile)	0.85	2.57	3.24	1.12
5	Both plain cotton cloth and pile (cap of pile)	0.70	2.46	3.27	2.20

Based on the findings presented in Figure 5, it is evident that the lateral displacement variations at various measuring points on the slope surface (Point A at the slope top, Point B at the slope middle, Point C at the slope center, and Point D at the slope bottom) follow a consistent trend across the five conditions: condition 1 > condition 3 > condition 2 > condition 4 > condition 5. The trend of lateral displacement remains the same, slope center > bottom of slope > top of slope. With the increase in the vertical load, the lateral displacement of the slope surface for each condition increases, the increase of the lateral displacement of the measuring point in the slope increases, the trend of the lateral displacement of the measuring points on the slope surface is more obvious, and the maximum lateral displacement corresponding to the limit load of the five conditions are all at the middle of the slope.

At the ultimate load of 17.5 kN for the pure sand structure, the lateral displacements of the measured points at the top of the slope A, the measured point in the middle of the slope B, the measured point in the middle of the slope C, and the measured point at the bottom of the slope D are 3.94 mm, 8.93 mm, 8.34 mm, and 5.92 mm, respectively. The lateral displacements at point A at the top of the slope were reduced by 67%, 37%, 72%, and 44%, respectively; at point B in the middle of the slope by −14%, 37%, 64%, and 63%, respectively; at point B in the middle of the slope by −12%, 46%, 69%, and 71%, respectively; and at point D at the bottom of the slope by 58%, 68%, 86%, and 88%, respectively. A comparative analysis shows that, under the action of the vertical load, the slope surface of condition 1 gradually produces the deflection outward, “the lateral deformation at the top and bottom of the slope is small, and the lateral deformation in the middle of the slope is large”. Due to the friction between the horizontal reinforcement and sand, the lateral deformation of the soil body has a limiting effect, with the increase in load, the friction between the horizontal reinforcement and sand gradually increases, thus improving the structural capacity and overall stability, but due to the middle of the structure between the reinforcement and sand, friction is obviously less than the upper load, so the middle of the slope in condition 2 (with reinforcement without pile) is a larger deflection produced by the “bulging phenomenon”. In the condition 3 structure, the vertical stresses borne by the soil are smaller due to the compression of the piles and the exertion of the pile lateral frictional resistance, resulting in a smaller amplitude of deflection and overall lateral displacement of the slope. For condition 4 and condition 5, due to the anchoring effect of the pile on the horizontal reinforcement material, the deflection and overall lateral displacement amplitude of the slope surface are even smaller, showing the reinforcing effect of the synergistic effect of the vertical pile and the horizontal reinforcement material, which verifies the superiority of the reinforcing performance of the pile penetration reinforcement structure proposed in this paper. Due to the existence of pile cap, the pile cap can better adjust the load-transfer mode, so that the pile compression is more uniform, the pile side friction resistance and pile end resistance bear the load more reasonably, and the deflection of the slope surface in condition 5 is smaller than that in condition 4.

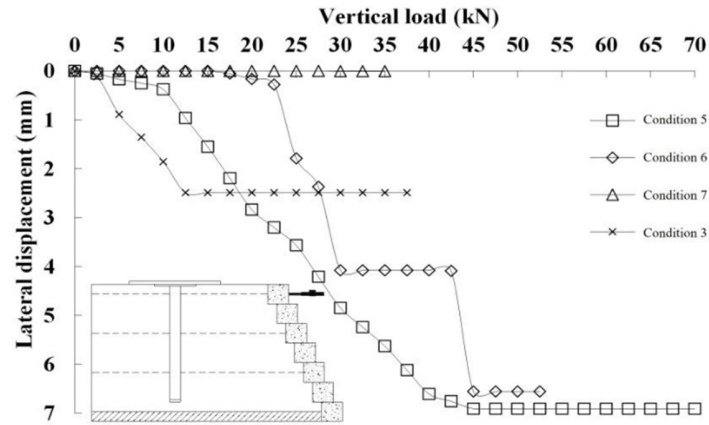
5.1.2. Effect of Different Reinforcement Layers

The vertical load–lateral displacement curves for the structure with varying numbers of reinforcement layers are presented in Figure 6. For Scenario 3, at the ultimate load of 35.0 kN, the corresponding lateral displacements for Scenarios 3, 7, 6, and 5 can be found in Table 8.

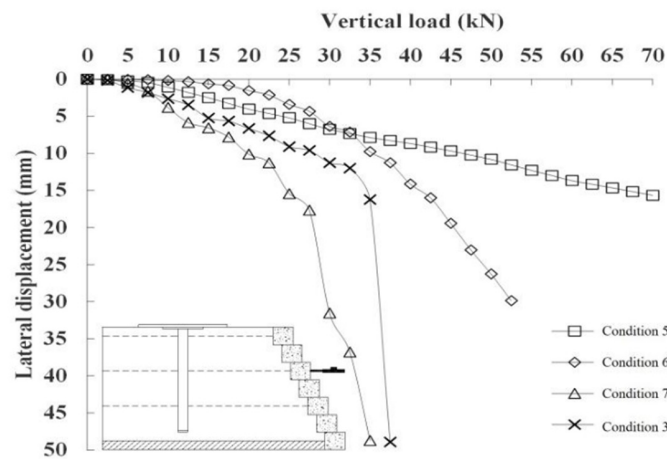
Based on the results in Figure 6a, it is clear that the lateral displacement of the pile penetrating the top of the reinforced structure increases with the increase in load in the initial loading stage.

From Figure 6b,c, it can be observed that the lateral displacement at the mid-point B, mid-point C, and bottom D of the structure increases with an increasing load. Additionally, the variation pattern across different conditions remains similar at these measurement points. In the initial and middle loading stages, the order of increase in lateral displacement is as follows: 1 layer of reinforcement > unreinforced > 3 layers of reinforcement > 2 layers

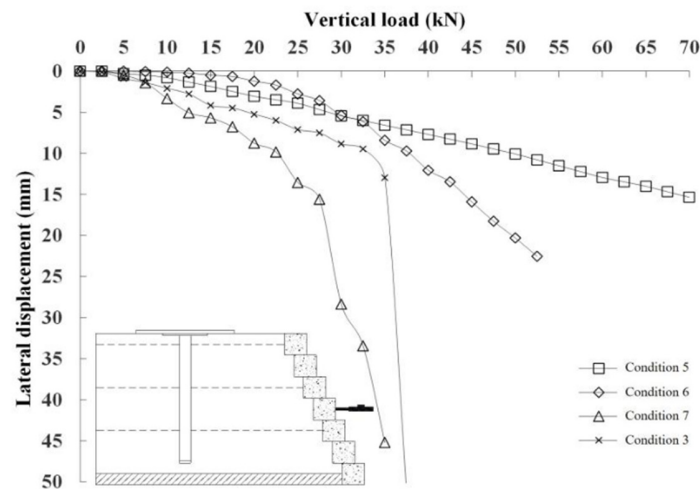
of reinforcement. However, in the later loading stage, the sequence of increased lateral displacement changes to the following: 1 layer of reinforcement > unreinforced > 2 layers of reinforcement > 3 layers of reinforcement. It is clear that increasing the number of reinforcement layers has a more pronounced effect in limiting lateral displacement in the later loading stages.



(a) Slope top A measurement point

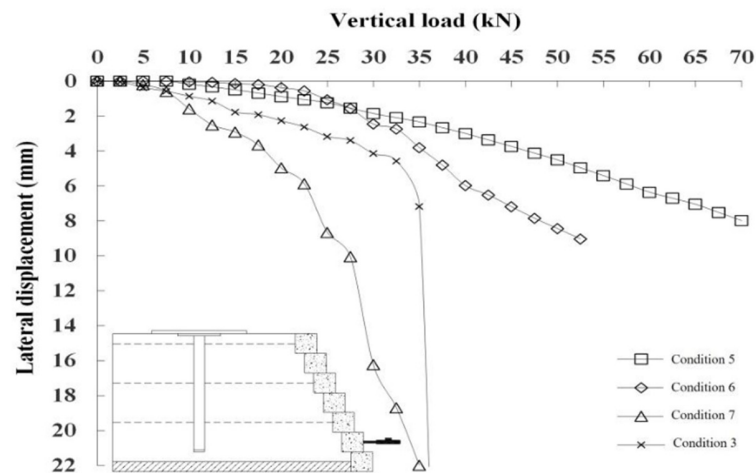


(b) B measurement point in slope



(c) C measurement point in slope

Figure 6. Cont.



(d) Slope D measurement point

Figure 6. Side displacement curve of different reinforced layers.

Table 8. Lateral displacement of different reinforced layer piles (Vertical load: 35.0 kN).

Condition	The Number of Reinforcement Layer n	Vertical Load Is the Horizontal Displacement Corresponding to 35.0 kN/mm			
		Slope Bottom D Station	In the Slope C Station	In the Slope B Station	Top of Slope A Station
3	0	7.18	12.98	16.25	2.49
7	1	21.98	45.21	48.73	0.01
6	2	3.81	8.42	9.77	4.08
5	3	2.34	6.58	7.87	5.63

As shown in Table 7, the results show that an appropriate increase in the number of layers of reinforcement laying can help to improve the overall stability, but the increase in the number of layers of reinforcement does not lead to a linear increase in the effect of reinforcement. It can be seen that, from the economic consideration, increasing the number of reinforcement layers will increase the structure cost of the project, so in the practical application, the needs of all parties should be taken into account, and then, the best reinforcement program should be formulated.

A comparison analysis between Figure 6 and Table 7 indicates that the addition of one layer of reinforcement at the bottom of the structure did not result in any significant restriction on the lateral displacement. However, the capacity to restrict lateral deformation significantly increased when two or three layers of reinforcement were added, compared to having no reinforcement.

5.1.3. Effects of Different Reinforcement Spacings

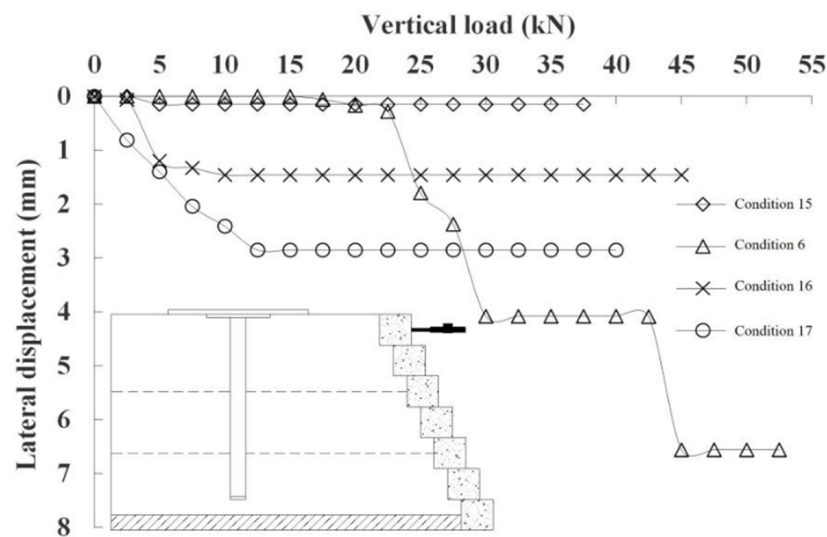
The term “reinforcement spacing” in this study refers to the distance between the second layer of reinforcement and the first layer, assuming that two layers of reinforcement are used, with the first layer fixed at the bottom of the structure. Figure 7 depicts the relationship curve between vertical load and lateral displacement for different reinforcement spacings in pile-supported reinforced structures. Table 9 provides the corresponding lateral displacements for various reinforcement spacings in structures under a vertical load of 32.5 kN.

From the observation in Figure 7a, it can be seen that in the early stage of loading, with the increase in load, the change rule of the incremental magnitude of lateral displacement at the top of the slope of the structure is basically the same, into the middle stage of loading, the incremental amount of lateral displacement at the top of the working condition 6 is

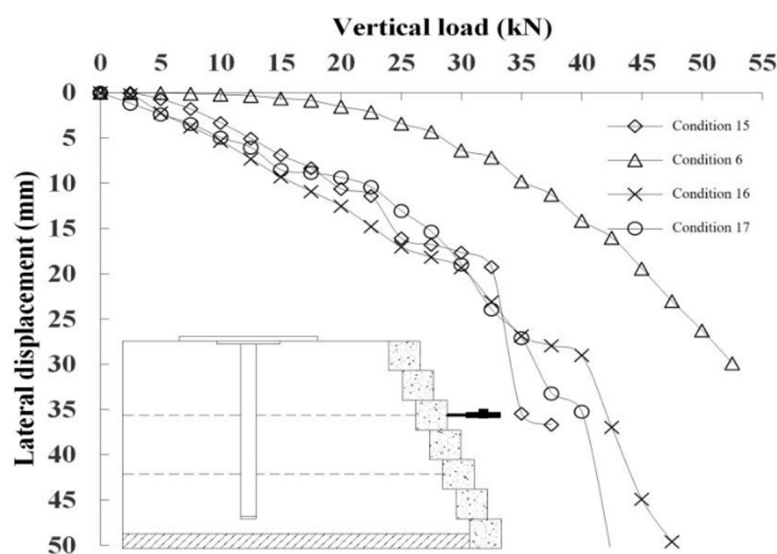
significantly increased, and the trend of the top lateral displacement tends to be stabilized after the loading is continued.

According to the results shown in Figure 7b, it can be seen that, when the vertical load is less than or equal to 32.5 kN, with the increase in the load, the change rule of the increase in the amount of lateral displacement of the B measurement point in the structure is similar under different working conditions.

From Figure 7c,d, it is evident that during the initial stages of loading, as the load increases, the lateral displacement increments at the C measurement point in the slope and the D measurement point at the bottom of the slope of this structure change in a nearly identical trend. A comprehensive analysis of Figure 7 and Table 9 shows that when the spacing between the 2nd layer of reinforcement and the 1st layer of reinforcement is 20 cm, the soil body is constrained by the larger reinforcement, and both the reinforcement and the soil body on the pro-slope face are damaged, but the misalignment is not obvious. This shows that a suitable spacing of reinforcement exists so that the lateral limiting effect of reinforcement on the soil can be maximized [13].

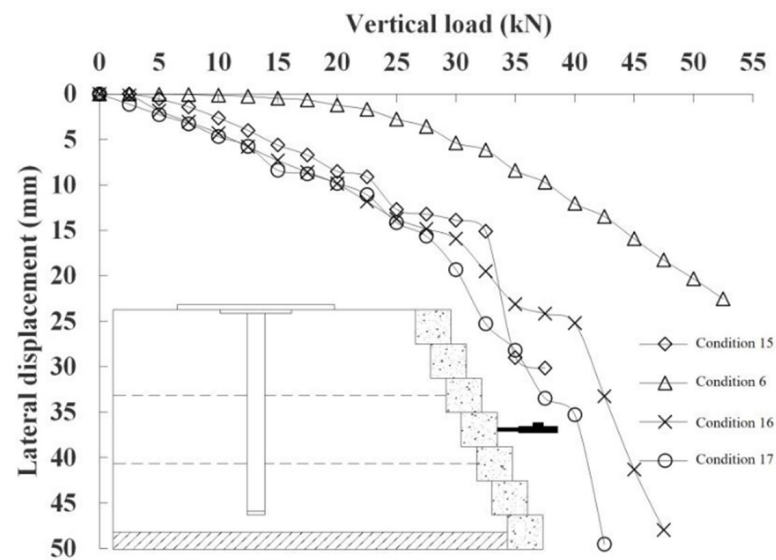


(a) Slope top A measurement point

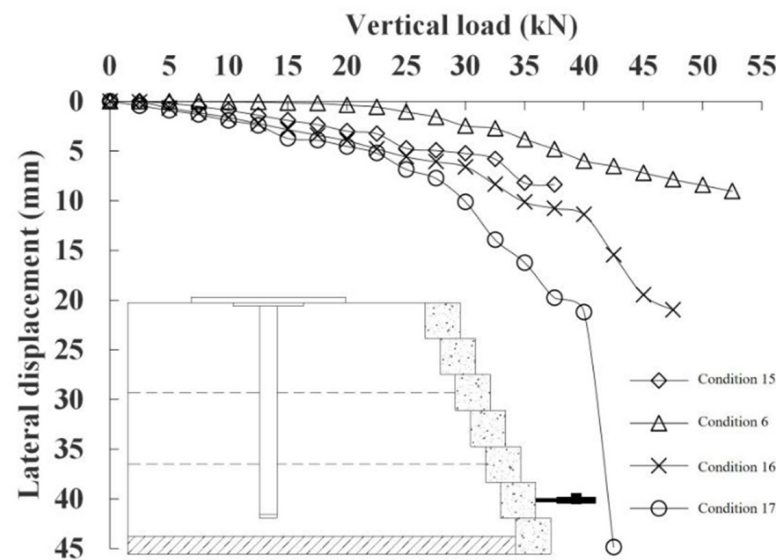


(b) B measurement point in slope

Figure 7. Cont.



(c) C measurement point in slope



(d) Slope D measurement point

Figure 7. Lateral displacement curve with different reinforcement spacings.

Table 9. Lateral displacement with different reinforcement spacings (vertical load: 32.5 kN).

Condition	Reinforcement Spacing/cm	Vertical Load Is the Horizontal Displacement Corresponding to 32.5 kN/mm			
		Slope Bottom D Station	In the Slope C Station	In the Slope B Station	In the Slope A Station
15	10	5.8	15.11	19.26	0.15
6	20	2.74	6.15	7.14	4.08
16	30	8.36	19.53	23.09	1.46
17	40	13.93	25.29	23.94	2.85

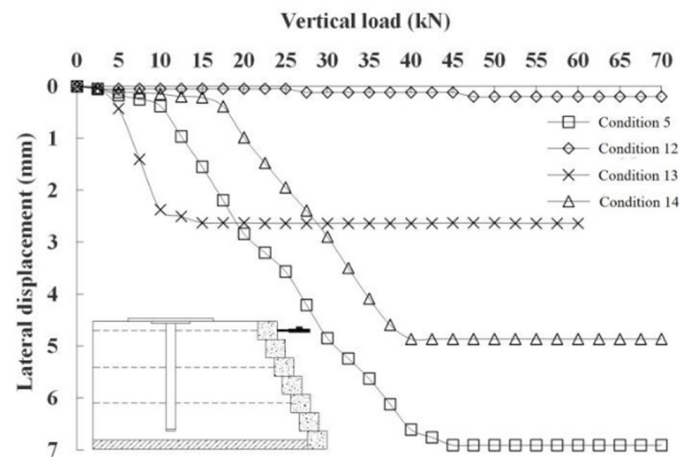
5.1.4. Effect of Different Pile Lengths

The vertical load–lateral displacement curves for structures with pile lengths of 50 cm, 55 cm, 60 cm, and 65 cm are shown in Figure 8.

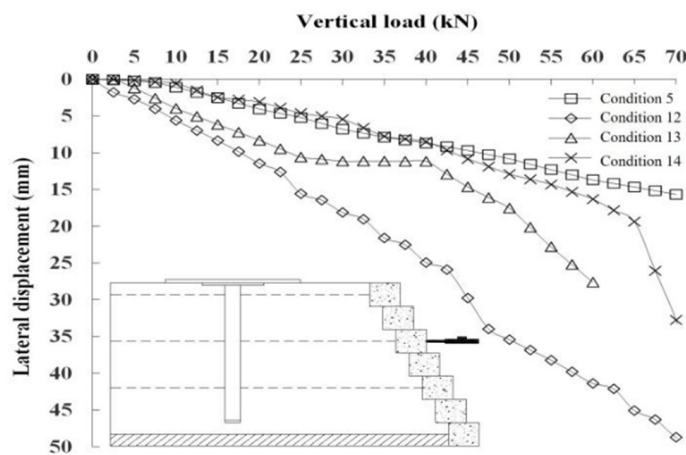
Based on the findings presented in Figure 8a, it is evident that when subjected to the same vertical load, the incremental change in lateral displacement at the crest of the structure follows a specific sequence: condition 13 > condition 5 > condition 14 > condition 12. In the intermediate loading phase, with the increase in load, there is minimal variation in lateral displacement at the crests for conditions 12 and 13, whereas conditions 5 and 14 show a distinct increase in lateral displacement. Moving into the later loading phase, as the load further escalates, the lateral displacement at the crest remains relatively stable across all conditions. Notably, the maximum lateral displacement at the crest aligns with the sequence: condition 5 > condition 14 > condition 13 > condition 12.

From the observations in Figure 8b–d, it can be seen that when the vertical load is greater than or equal to 40 kN, the lateral displacement trends of the middle and bottom of this structure are relatively the same. However, when the vertical load exceeds 40 kN, the lateral displacement trends in the middle and bottom of the structure are similar with an increasing load: condition 12 > condition 13 > condition 14 > condition 5.

The findings from Figure 8 and Table 10 demonstrate that increasing the pile length within a specific range improves the ability of the structure to limit lateral displacement at the midsection and base [28].

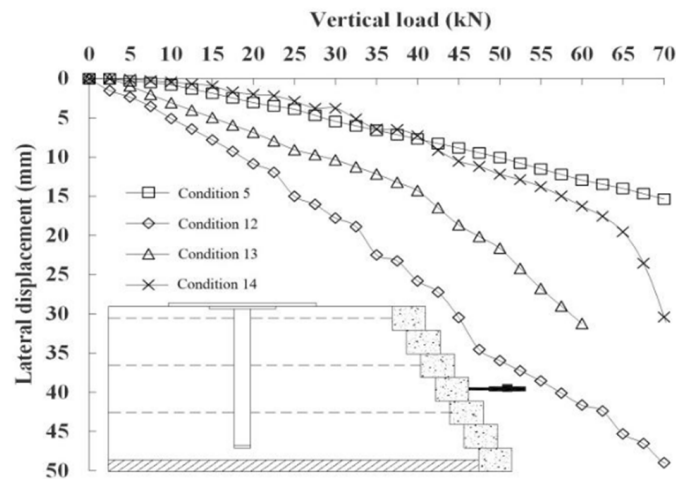


(a) Slope top A measurement point

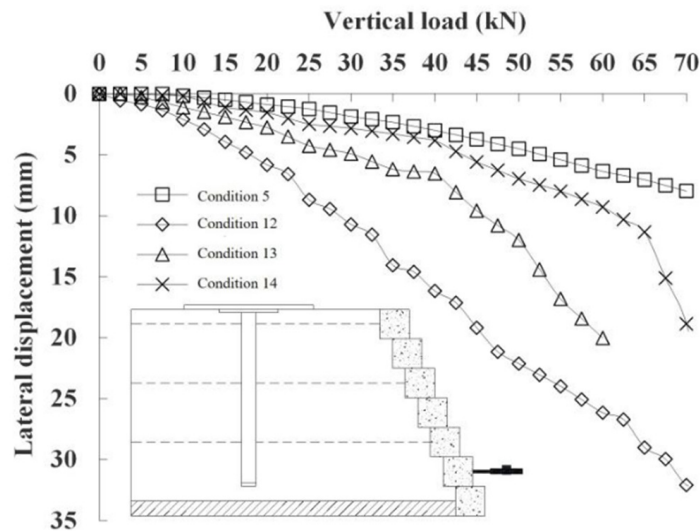


(b) B measurement point in slope

Figure 8. Cont.



(c) C measurement point in slope



(d) Slope D measurement point

Figure 8. Lateral displacement curve of vertical load of reinforced fill structure with pile penetration of different long piles.

Table 10. Lateral displacement of penetrating reinforced constructions with different long piles (vertical load: 55.0 kN).

Condition	Pile Length/cm	Ultimate Bearing Capacity Q/kN	Horizontal Displacement Amount Corresponding to the Ultimate Bearing Capacity/mm			
			Slope Bottom D Station	In the Slope C Station	In the Slope B Station	In the Slope A Station
12	50	55.0	23.99	38.56	38.23	0.20
13	55	60.0	16.83	26.77	22.79	2.64
5	60	70.0	5.41	11.51	12.30	6.91
14	65	60.0	7.99	13.78	14.31	4.86

5.2. The Distribution Law of Pile-Bending Moments

The pile-bending moment is a direct reflection of the working condition of the reinforcing members and helps in the study of the reinforcement mechanism. In order to determine the bending moments (M_i) at various sections of the pile, experimental measurements of

tensile and compressive strains (ϵ_t and ϵ_c) at specific measurement points along the pile section are utilized. This calculation is carried out using the bending theory, as described in Equation (1) [18,23],

$$M_i = EI\Delta\epsilon/d \quad (1)$$

The equation includes the following parameters: E , which represents the elastic modulus of the model pile; I , which denotes the moment of inertia of the pile section; $\Delta\epsilon$, which signifies the bending strain of the pile section; and d , which stands for the distance between two measurement points, equivalent to the pile diameter (m).

5.2.1. Impact of Different Structure Types

The bending moment distribution curve of pile of each structure type is shown in Figure 9. The maximum bending moments of the pile for different structural types are listed in Table 11.

Table 11. Maximum bending moment value of the pile for different structure types.

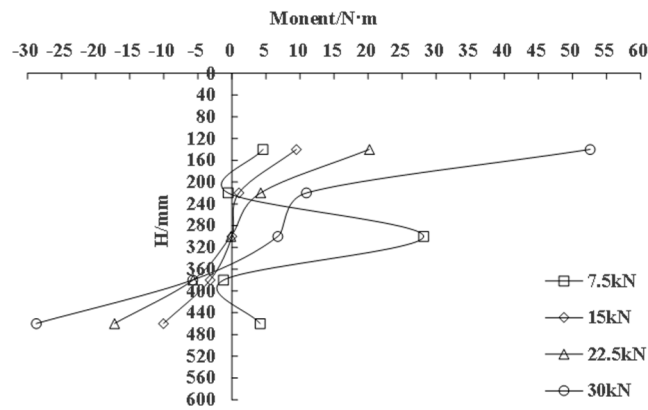
Condition	Structure Type	Maximum Bending Moment/(N·m)	Vertical Load/kN	Pile Depth/mm
1	Sand	-	-	-
2	Flat grain cotton cloth	-	-	-
3	Pile	52.61	30.0	140
4	Both plain cotton cloth and pile (no cap of pile)	42.89	45.0	140
5	Both plain cotton cloth and pile (cap of pile)	26.11	67.5	300

According to the observation in Figure 9a, it can be seen that when the vertical load is large, the maximum positive bending moment occurs near the top of the pile, the positive bending moment of the pile decreases along the depth direction, and after reaching the zero point, the negative bending moment of the pile increases along the depth direction of the pile, and the bending moment of the pile shows that the distribution of “the upper part of the bending moment is positive, and the lower part of the bending moment is negative”, which is basically the same as that of the distribution of the bending moments for foundation piles of bridges on high steep slopes [23,29].

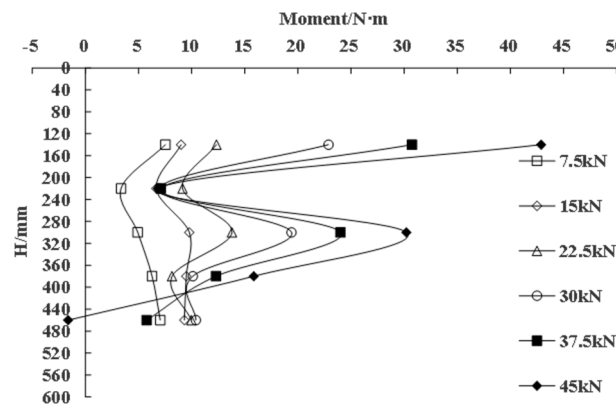
Based on the results shown in Figure 9b, it is evident that high positive bending moments are observed in both the upper and lower parts of the pile during the initial loading stage. As the loading entered the middle stage, the positive bending moments in the upper portion remained elevated, while there was a significant increase in the middle portion, which peaked at a depth of 300 mm. The smallest bending moments were observed at the depths of 220 mm and 380 mm. In the final stage of loading, the positive bending moments in both the upper and middle portions of the pile increased significantly as the load increased, while the positive bending moments in the upper portion increased more.

The analysis in Figure 9c shows that the bending moments gradually increase between 140 and 300 mm and then decreased between 300 and 460 mm, peaking at 300 mm. In addition, their bending moments were higher with an increasing load, which was particularly evident at a depth of 300 mm.

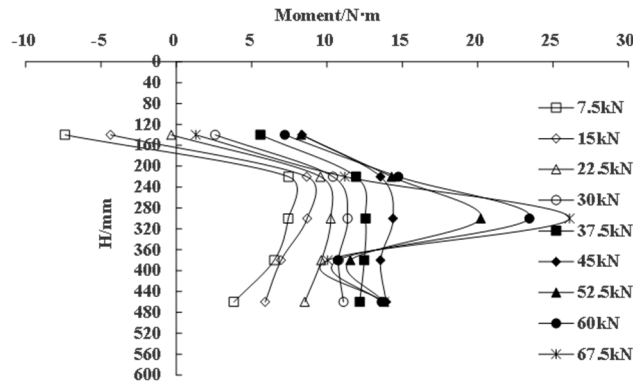
The analysis of Figure 9 and Table 10 reveals that structures with only piles are prone to rotational deformation around the pile end under vertical loads due to the lack of lateral restraint by the horizontal reinforcement material. The structure with flat grain cotton cloth and pile (without the cap of the pile) mainly produces flexural deformation of the pile due to the lateral restraint of the horizontal reinforcement material when the load is small. At higher loads, the rotational deformation of the pile around the pile end is obvious. For the structure with flat grain cotton cloth and a pile (with cap of pile), the cap of the pile enhances the ability to limit the lateral displacement of the top of the pile and makes the bending moment distribution of the pile more reasonable [30].



(a) Moment distribution diagram of pile in working condition 3



(b) Moment distribution diagram of pile in working condition 4



(c) Moment distribution diagram of pile in working condition 5

Figure 9. Moment distribution diagram of pile.

5.2.2. Effect of Different Pile Lengths

Figure 10 illustrates the variation in pile-bending moments for pile lengths of 50 cm, 55 cm, 60 cm, and 65 cm in the structure. Table 12 presents the maximum pile bending moments for different pile lengths in the structure.

Based on Figure 10a,b, it can be observed that the trend in pile-bending moments is quite similar for shorter pile lengths. Initially, between depths of 140 and 300 mm, the pile-bending moment gradually increases with depth. However, between depths of 300 and 380 mm, there is a decrease in the bending moment, followed by an increase between depths of 380 and 460 mm. Therefore, the largest bending moments occur at depths of 300 mm and 460 mm. In the mid and later stages of loading, as the load increases, the bending moment at a depth of 140 mm experiences a noticeable and significant increase.

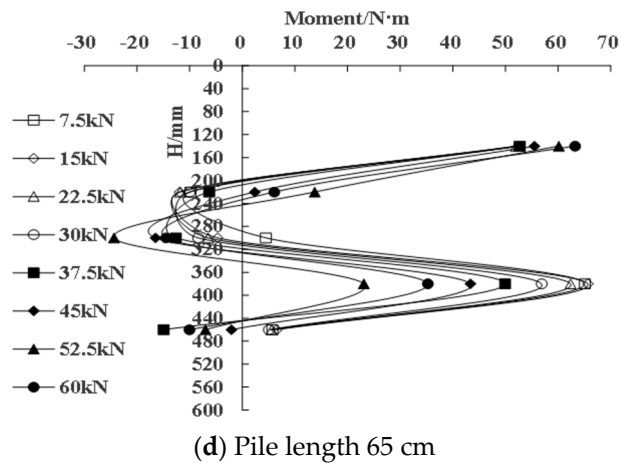
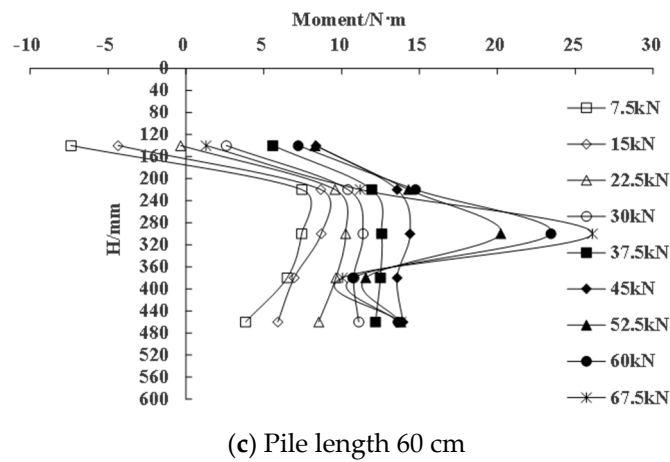
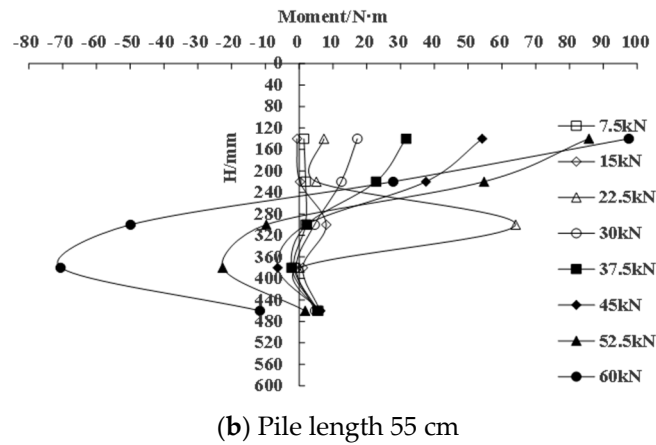
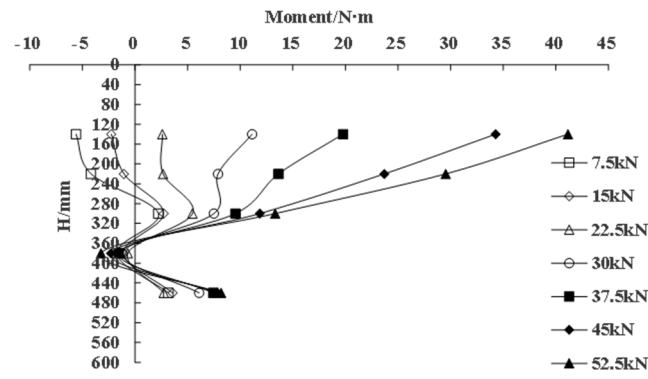


Figure 10. Change diagram of the bending moment of reinforced structures with different long piles.

Table 12. Maximum bending moment of reinforced fill structure with pile penetration.

Condition	Pile Length/cm	Maximum Bending Moment/(N·m)	Vertical Load/kN	Pile Depth/mm
12	50	41.16	52.5	140
13	55	97.51	60.0	140
5	60	26.11	67.5	300
14	65	63.22	60.0	140

Upon analyzing Figure 10c, it can be observed that for a pile length of 60 cm, the distribution of the pile-bending moments exhibits a parabolic trend with the depth. The maximum moment is found at a depth of 300 mm.

Based on Figure 10d, it can be observed that for a pile length of 65 cm, the pile-bending moment shows different trends at different depths. On the other hand, between depths of 300 and 460 mm, the distribution follows a parabolic trend with depth. When the vertical load is relatively low, the maximum pile-bending moment is found at a depth of 300 mm and decreases as the load increases. However, with higher vertical loads, the maximum bending moment occurs at a depth of 140 mm and increases with the load.

By combining Figure 10 and Table 12, it can be inferred that with the increase in the pile length, the corresponding position of the maximum bending moment of the pile is shifted downward from the upper part to the middle part, and the corresponding position of the zero point of the bending moment is shifted downward. This shows that when the pile length is short, the embedment depth of the pile is small, and the bending moment of the pile is mainly caused by the rotational deformation of the pile under the action of a large vertical load. When the pile length is longer, the embedment depth of the pile is larger, which provides sufficient resistance to the rotational deformation of the pile, and the bending moment of the pile is mainly caused by the flexural deformation of the pile under the action of a larger vertical load [31].

5.2.3. Effect of Different Numbers of Reinforcement Layers

The plot in Figure 11 illustrates the distribution of the bending moment along the pile for various numbers of reinforcement layers. Table 13 displays the maximum bending moment values for the structure with different numbers of reinforcement layers.

From Figure 11a, it can be observed that in the absence of reinforcement, the bending moment distribution along the pile increases parabolically with depth during the initial loading.

According to Figure 11b, the addition of a single layer of horizontal reinforcement at the base results in a linear decrease in the bending moment with a depth in the range of 140–220 mm, for a relatively small vertical load. However, from a depth of 220 mm to 460 mm, the bending moment distribution follows a parabolic pattern. When the vertical load reaches 30.0 kN, both the negative bending moment in the upper part and the positive bending moment in the lower part increase to their maximum values.

According to Figure 11c, when two layers of horizontal reinforcement are added, the bending moment decreases nonlinearly with depth from 140–300 mm for vertical loads ≤ 30.0 kN. After that, it follows a parabolic distribution from a 300 mm to 460 mm depth, with the maximum bending moment occurring at a 380 mm depth. However, when the vertical load exceeds 30.0 kN, there is a significant increase in both the positive bending moment in the upper part and in the negative bending moment in the lower part.

In Figure 11d, the addition of three layers of horizontal reinforcement leads to a parabolic pattern in the bending moment distribution along the depth of the pile. This results in a more reasonable distribution of the bending moment, with the maximum bending moment of 26.11 N·m occurring at a depth of 300 mm.

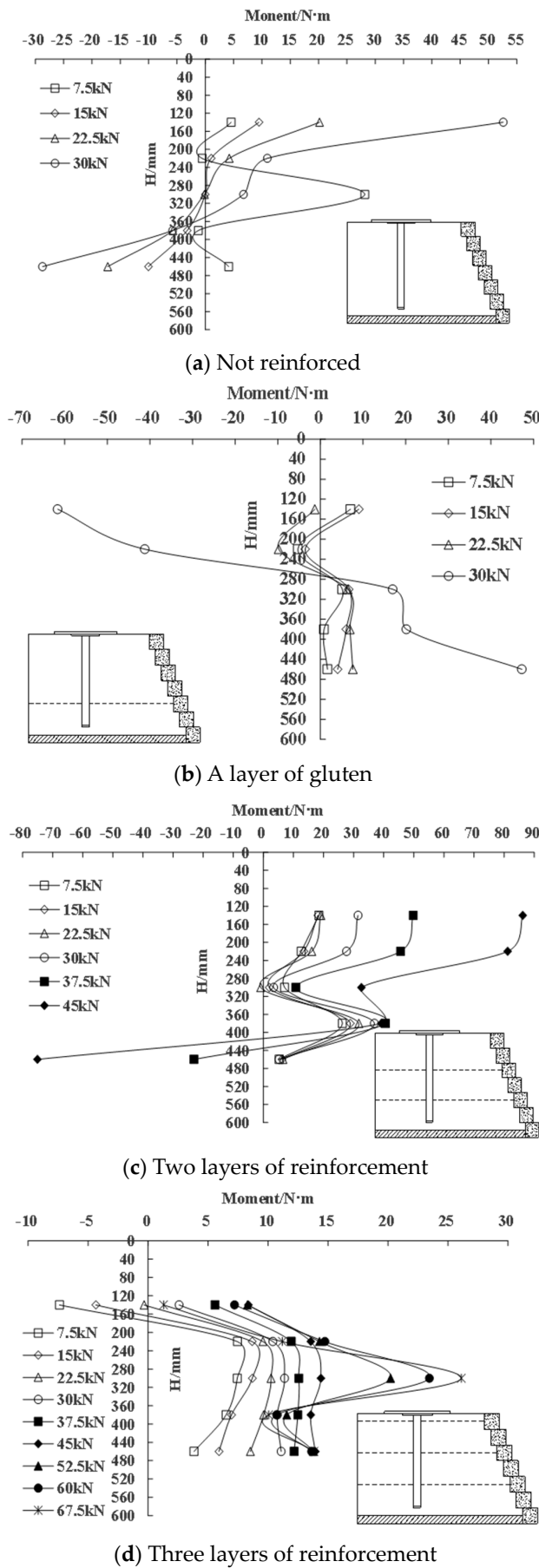


Figure 11. Moment distribution diagram of reinforced piles with different reinforced layers.

Table 13. Maximum bending moment values with different reinforced layers.

Condition	The Number of Reinforcement Layer n	Maximum Bending Moment/(N·m)	Vertical Load/kN	Pile Depth/mm
3	0	52.61	30.0	140
7	1	−61.64	30.0	140
6	2	86.19	45.0	140
5	3	26.11	67.5	300

5.2.4. Effects of Different Slope Rates

Figure 12 illustrates the variation in the bending moment along the pile of the pile for slope ratios of 0.6, 0.4, and 0.2. Table 14 presents the values of the maximum bending moments for the structure at different slope ratios.

In Figure 12a, it can be observed that when the slope ratio is 0.6, the bending moment along the pile decreases nonlinearly with depth within the range of 140–300 mm during the early and middle stages of loading. From a depth of 300 mm to 460 mm, the bending moment follows a parabolic trend. In the later stages of loading, as the load increases, there is a significant increase in the bending moment below a depth of 220 mm in the pile. This deformation pattern exhibits only positive bending moments, similar to the passive load-bearing mode of a cantilever structure. The maximum bending moment of 59.85 N·m is observed at a depth of 380 mm, which closely resembles the distribution pattern of bending moments in a single vertical pile of a micro-pile reinforced earth retaining wall [32].

According to Figure 12b, the bending moment distribution along the pile follows a parabolic trend with depth, with a slope ratio of 0.4. The maximum bending moment of 26.11 N·m is observed at a depth of 300 mm.

Based on Figure 12c, a slope ratio of 0.2 and loading in the middle and later stages result in a point of inflection at a depth of 340 mm along the pile, where the bending moment becomes zero. Above this point, a parabolic distribution of bending moments is observed on both sides. The bending moment in the pile is positive above the inflection point (bending in the same direction as soil sliding), while it is negative below the inflection point (bending in the opposite direction to soil sliding). This bending moment behavior resembles that of a micro-pile reinforced earth retaining wall [18,19,22]. With an increasing load, the positions of the maximum bending moment and the inflection point remain relatively constant, but the magnitude of the bending moment increases significantly, reaching a peak of 115.88 N·m.

The analysis of Figure 12 and Table 14 reveals that the slope ratio has a significant effect on the distribution of the bending moments during the middle and later stages of loading. Within a certain range, reducing the slope ratio can decrease the maximum bending moment, leading to a more reasonable distribution of bending moments in the pile and preventing localized stress concentrations in the pile. However, if the slope ratio is too small, the absolute magnitude of the bending moment increases.

Table 14. Maximum bending moment value of structures with different slope rates.

Condition	Ratio of Slope	Maximum Bending Moment/(N·m)	Vertical Load/kN	Pile Depth/mm
9	0.6	59.85	45.0	380
5	0.4	26.11	67.5	300
8	0.2	115.88	52.5	220

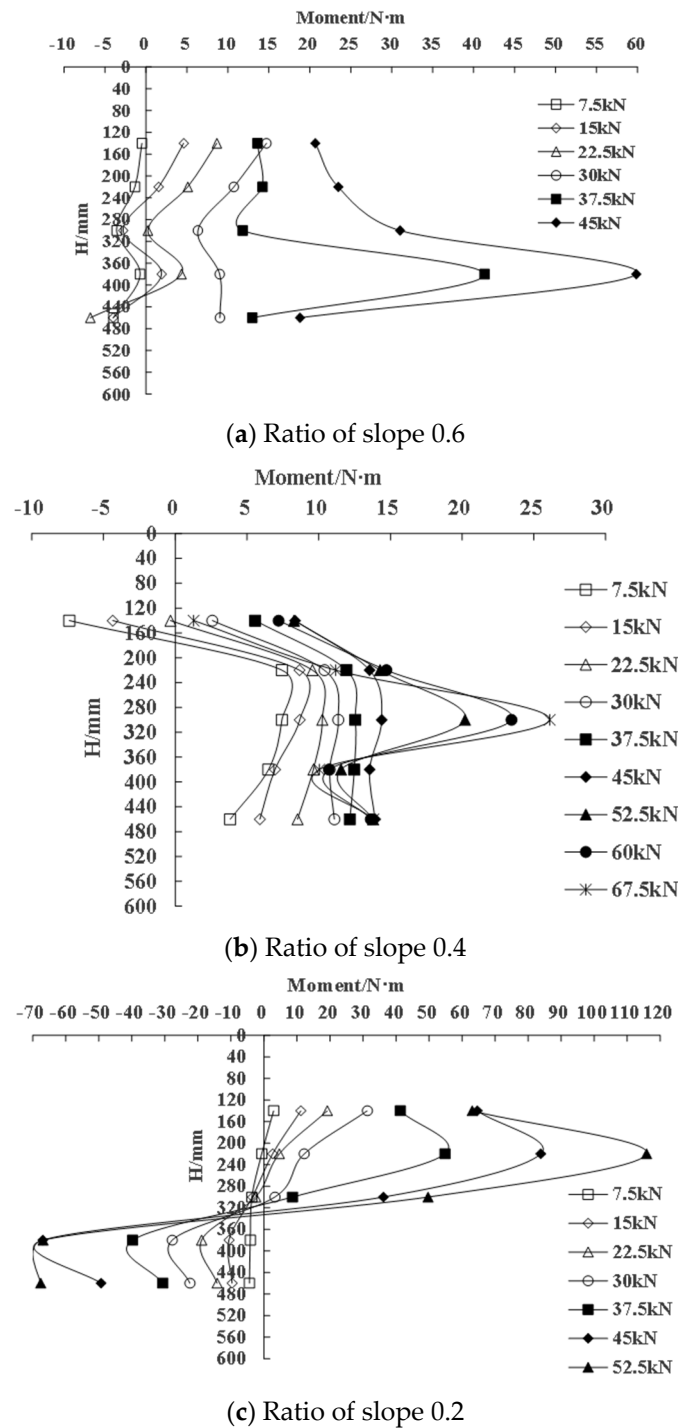


Figure 12. Change diagram of bending moment of reinforced piles with different slope rates.

6. Conclusions

This study was on the bearing and reinforcement characteristics of a pile-penetrating reinforced structure through an indoor model test. The study yielded the following main conclusions:

- (1) By measuring the lateral displacements of the soil on the slope we can find that the reinforced fill structure with pile penetration enhances the ability to limit lateral displacement through the synergistic effect of vertical piles, the cap of piles, and horizontal reinforcement. This results in a more reasonable distribution of the bending moment in the pile and improved distribution of the vertical earth pressure.

- (2) Increasing the pile length and the number of reinforcement layers within a certain range enhances the effect of limiting lateral displacements in the middle and at the bottom of the slope of the reinforced fill structure with pile penetration. This reduces the extreme value of the bending moment and makes the distribution of the bending moment in the pile more uniform. The appropriate spacing of the reinforcement maximizes the lateral confinement effect on the soil body.
- (3) Within a certain range, decreasing the slope rate reduces the extreme value of the bending moment, improves the distribution of the bending moment in the pile, and avoids localized force concentration. However, if the slope rate is too small, the absolute amplitude of bending moment increases. Moreover, increasing the pile diameter significantly reduces the vertical soil pressure below the cap of pile and between the cap of piles.

Author Contributions: Q.M.: Funding acquisition, Supervision, Data curation. H.Y.: Formal analysis, Writing—original draft, Investigation, Visualization. Y.Y.: Conceptualization, Methodology, Writing—review & editing, Investigation. L.X.: resources. All authors have read and agreed to the published version of the manuscript.

Funding: The authors are grateful for the financial support of the National Natural Science Foundation of China (Grant Nos. 52078194), the National Young Top-notch Talent of “Ten Thousand Talents Program”, the Science Fund for Distinguished Young Scholars of Hubei Province (2022CFA043), the Young Top-notch Talent Cultivation Program of Hubei Province, the Outstanding Young and middle-aged Science and Technology Innovation Team of colleges and universities in Hubei Province (No. T2022010), and the Innovation Demonstration Base of Ecological Environment Geotechnical and Ecological Restoration of Rivers and Lakes (No. 2020EJB004).

Institutional Review Board Statement: Not applicable.

Informed Consent Statement: Not applicable.

Data Availability Statement: The raw data supporting the conclusions of this article will be made available by the authors on request.

Conflicts of Interest: Author Yicong Yang was employed by the company Sinohydro Bureau 8 Co., Ltd. The remaining authors declare that the research was conducted in the absence of any commercial or financial relationships that could be construed as a potential conflict of interest.

References

1. Wang, Y.Y.; Sang, S.K.; Zhang, M.Y.; Jeng, D.S.; Yuan, B.X.; Chen, Z.X. Laboratory study on pile jacking resistance of jacked pile. *Soil Dyn. Earthq. Eng.* **2022**, *154*, 107070. [[CrossRef](#)]
2. Sales, M.M.; Prezzi, M.; Salgado, R. Load-settlement behaviour of model pile groups in sand under vertical load. *J Civ Eng Manag* **2017**, *23*, 1148–1163. [[CrossRef](#)]
3. Luan, L.; Ding, X.; Cao, G.; Deng, X. Development of a coupled pile-to-pile interaction model for the dynamic analysis of pile groups subjected to vertical loads. *Acta Geotech.* **2020**, *15*, 3261–3269. [[CrossRef](#)]
4. Luan, L.; Deng, X.; Deng, W.; Wang, C.; Ding, X. Influence of pile geometry on responses of end-bearing pile groups subjected to vertical dynamic loads. *Int. J. Struct. Stab. Dyn.* **2020**, *20*, 2050050. [[CrossRef](#)]
5. Sang, Y.; Yu, S.; Wang, Z.; Zhao, H. The loading test on the single pile with cap of pile in transparent soil model. *ASTM Int.* **2019**, *42*, 20170153. [[CrossRef](#)]
6. Ding, X.; Zhang, T.; Li, P.; Cheng, K. A theoretical analysis of the bearing performance of vertically loaded large-diameter pipe pile groups. *J. Ocean. Univ. China* **2016**, *15*, 57–68. [[CrossRef](#)]
7. Yuan, B.; Chen, R.; Teng, J.; Peng, T.; Feng, Z. Effect of passive pile on 3D ground deformation and on active pile response. *Sci. World J.* **2014**, *2014*, 904186. [[CrossRef](#)]
8. Wei, L.; Zhang, K.; He, Q.; Zhang, C. Mechanical Response Analysis for an Active–Passive Pile Adjacent to Surcharge Load. *Appl. Sci.* **2023**, *13*, 4196. [[CrossRef](#)]
9. Yang, M.; Shangguan, S.; Li, W.; Zhu, B. Numerical study of consolidation effect on the response of passive piles adjacent to surcharge load. *Int. J. Geomech.* **2017**, *17*, 04017093. [[CrossRef](#)]
10. Zomorodian, S.M.A.; Dehghan, M. Lateral resistance of a pile installed near a reinforced slope. *Int. J. Phys. Model. Geotech.* **2011**, *11*, 156–165. [[CrossRef](#)]
11. Pierson, M.C.; Parsons, R.L.; Han, J.; Brennan, J.J. Capacities and deflections of laterally loaded shafts behind an MSE wall. *Transp. Res. Rec.* **2009**, *2116*, 62–69. [[CrossRef](#)]

12. Sawwaf, E.M. Lateral resistance of single pile located near geosynthetic reinforced slope. *J. Geotech. Geoenviron. Eng.* **2006**, *132*, 1336–1345. [[CrossRef](#)]
13. Yoo, C. Laboratory investigation of bearing capacity behavior of strip footing on geogrid-reinforced sand slope. *Geotext. Geomembr.* **2001**, *19*, 279–298. [[CrossRef](#)]
14. Sommers, A.N.; Viswanadham, B.V.S. Centrifuge Model Tests on The Behavior of Strip Footing on Geotextile-Reinforced Slopes. *Geotext. Geomembr.* **2009**, *27*, 497–505. [[CrossRef](#)]
15. Choudhury, A.K.; Jha, J.N.; Gill, K.S. Laboratory investigation of bearing capacity behavior of strip footing on reinforced flaysh slope. *Geotext. Geomembr.* **2010**, *28*, 393–402. [[CrossRef](#)]
16. Raisinghani, D.V.; Viswanadham, B.V.S. Centrifuge model study on low permeable slope reinforced by hybrid geosynthetics. *Geotext. Geomembr.* **2011**, *29*, 567–580. [[CrossRef](#)]
17. Gill, K.S.; Choudhary, A.K.; Jha, J.N.; Shukla, S.K. Experimental and numerical studies of loaded strip footing resting on reinforced fly ash slope. *Geosynth. Int.* **2013**, *20*, 13–25. [[CrossRef](#)]
18. Song, F.; Liu, H.; Ma, L.; Hu, H. Numerical analysis of geocell-reinforced retaining wall failure modes. *Geotext. Geomembr.* **2018**, *46*, 284–296. [[CrossRef](#)]
19. Zhang, Z.C.; Pak, R.Y.S.; Chen, Y.M.; Liu, H.L. Study on the performance of the micropile-mechanically stabilized earth wall. *J. Mt. Sci.* **2018**, *15*, 825–844. [[CrossRef](#)]
20. Gao, L.; Wang, K.; Xiao, S.; Wu, W. Dynamic response of a pile considering the interaction of pile variable cross section with the surrounding layered soil. *Int. J. Numer. Anal. Methods Geomech.* **2017**, *41*, 1196–1214. [[CrossRef](#)]
21. Ye, J.; He, X. Evaluation of flexural stiffness on mechanical property of dual row retaining pile wall. *Mech. Adv. Mater. Structures* **2022**, *29*, 963–974. [[CrossRef](#)]
22. Hossain, M.Z.; Abedin, M.Z.; Rahman, M.R.; Haque, N.; Jadid, R. Effectiveness of sand compaction piles in improving loose cohesionless soil. *Transp. Geotech.* **2021**, *26*, 100451. [[CrossRef](#)]
23. Liu, J.; Zhao, M.; Yang, M. Experimental study on the model of bridge foundation pile on high and steep rock slope. *J. Geotech. Eng.* **2009**, *31*, 372–377.
24. Lakomski, M.; Tosik, G.; Niedzielski, P. Optical fiber sensor for PVC sheet piles monitoring. *Electronics* **2021**, *10*, 1604. [[CrossRef](#)]
25. Pan, C.; Yang, M.; Shanguan, S.; Li, W. Material properties of piles or beams in physical model tests and the basis for selection. *Struct. Eng.* **2018**, *34*, 135–141. [[CrossRef](#)]
26. Zheng, J.; Nie, C.; Lu, Y. Analytical solution of the column hole expansion problem based on the soil plug effect. *J. Rock Mech. Eng.* **2006**, *25* (Suppl. S2), 4004–4008.
27. *JGJ 106-2014*; Technical Specification for Building Foundation Pile Detection. China State Engineering and Construction Press: Beijing, China, 2014.
28. Wang, Y.; Sang, S.; Liu, X.; Huang, Y.; Zhang, M.; Miao, D. Model test of jacked pile penetration process considering influence of pile diameter. *Front. Phys.* **2021**, *9*, 616410. [[CrossRef](#)]
29. Zhao, H.; Yin, P.; Li, X. Mechanical response of bridge piles in high-steep slopes and sensitivity study. *J. Cent. South Univ.* **2015**, *22*, 4043–4048. [[CrossRef](#)]
30. Zhang, J.; Wei, K.; Li, J. Integrated assessment of the hydrodynamic added mass of the deep-water pile-cap foundation considering pile group-cap of pile interaction. *Ocean. Eng.* **2022**, *244*, 110418. [[CrossRef](#)]
31. Kim, S.; Whang, S.W.; Kim, S. Pile foundation design through the increased bearing capacity of extended end pile. *J. Asian Archit. Build. Eng.* **2017**, *16*, 395–402. [[CrossRef](#)]
32. Tang, X.S.; Zheng, Y.R.; Xin, J.P. Experimental study and numerical simulation on the large-sized models of micro anti-slide piles. *Adv. Mater. Res.* **2014**, *919*, 670–677.

Disclaimer/Publisher’s Note: The statements, opinions and data contained in all publications are solely those of the individual author(s) and contributor(s) and not of MDPI and/or the editor(s). MDPI and/or the editor(s) disclaim responsibility for any injury to people or property resulting from any ideas, methods, instructions or products referred to in the content.